RESEARCH PAPER

# Comparative SEM–EDX analysis of intestinal calcium deposition in a teleost (*Sardinella longiceps*) and an elasmobranch (*Rhinobatos annandalei*): implications for marine carbonate cycling and coral reef ecosystems

**Jeyapraba L, Paul Sweetlin P, Sofia Revathy K, Nirmala S and Viji Margaret.I**

Department of Zoology and Research Centre, Sarah Tucker College (Autonomous), Affiliated to Manonmaniam Sundaranar University, Tirunelveli – 627007, Tamil Nadu, India

*Corresponding author: jayaprabha2009@gmail.com

Received: 25th Aug, 2026 | Revised: 1st Sep, 2026 | Accepted: 5th Sep, 2026 | Available Online: 7th Oct, 2026

**ABSTRACT**

Marine teleosts precipitate carbonate minerals in their intestines and excrete them, and these precipitates contribute an estimated 3–15% of oceanic carbonate production. Whether elasmobranchs form comparable deposits is almost unknown. This study compared the morphology and elemental composition of solid material recovered from the intestinal fluid of a teleost, the Indian oil sardine (*Sardinella longiceps*), and an elasmobranch, the Bengal guitarfish (*Rhinobatos annandalei*). Intestinal fluid was filtered, and the retained material was oven-dried and analysed by scanning electron microscopy with energy-dispersive X-ray spectroscopy (SEM–EDX). Calcium was detected in both deposits. The ray-fish deposit contained 27.47 wt.% calcium (15.27 at.%), 2.32 times the 11.82 wt.% (6.22 at.%) of the sardine deposit; the difference of 15.65 ± 2.21 percentage points was about seven times the combined analytical uncertainty. The ray-fish deposit was also richer in phosphorus (14.62 vs. 6.83 wt.%), whereas the sardine deposit was dominated by silicon (21.65 vs. 3.52 wt.%) and contained aluminium (7.82 wt.%). SEM showed rosettes of spindle-shaped crystallites and ovoid granules in the ray-fish deposit, and diatom frustules in the sardine deposit. Ca/P atomic ratios (1.45 and 1.34) were consistent with calcium phosphate, while the ray-fish deposit alone held oxygen in excess of oxide stoichiometry (15.1 at.%), consistent with an additional carbonate or hydrated phase. These results provide a first elemental comparison of teleost and elasmobranch intestinal deposits and identify the mineral-phase and replicated analyses needed to assess the role of elasmobranchs in marine carbonate cycling.

**Key words:** intestinal carbonate, elasmobranch, *Sardinella longiceps*, *Rhinobatos annandalei*, SEM–EDX, calcium, marine carbonate cycle

**How to cite this article:** Jeyapraba L, Paul Sweetlin P, Sofia Revathy K, Nirmala S, Viji Margaret.I. Comparative SEM–EDX analysis of intestinal calcium deposition in a teleost (Sardinella longiceps) and an elasmobranch (Rhinobatos annandalei): implications for marine carbonate cycling and coral reef ecosystems. Int J Drug Deliv Technol. 2026;16(89s):224-231. DOI: 10.25258/ijddt.16.89s.22.

## 1. INTRODUCTION

Oceanic calcium carbonate production has traditionally been attributed to coccolithophores, foraminifera, corals and molluscs. Wilson *et al.* (2009) showed that marine teleosts also precipitate carbonate in their intestines and excrete it, and estimated that fishes contribute 3–15% of total oceanic carbonate production. Fish carbonates are rich in magnesium and more soluble than most other biogenic carbonates, which may influence alkalinity in the upper ocean (Wilson *et al.*, 2009). In the Bahamas, fishes produce about $6.1 \times 10^6$ kg of carbonate a year, roughly 14% of total carbonate mud production (Perry *et al.*, 2011).

The process is a by-product of osmoregulation. Marine teleosts drink seawater to replace water lost by osmosis and secrete bicarbonate into the intestine; the resulting alkaline fluid precipitates calcium and magnesium as carbonate, which lowers luminal osmolality and aids water absorption (Wilson & Grosell, 2003; Whittamore *et al.*, 2010). The precipitates can be amorphous: in the gilt-head seabream (*Sparus aurata*) they form a stable amorphous calcium carbonate containing up to 54 mol% magnesium (Foran *et al.*, 2013). Across 22 Bahamian species, high-magnesium calcite dominated, with smaller amounts of calcite, amorphous carbonate and aragonite (Salter *et al.*, 2017). The pellets show distinctive crystal morphologies (Salter *et al.*, 2014), and among reef fishes excretion rate is best predicted by body mass and relative intestine length, while mineralogy is conserved within families (Ghilardi *et al.*, 2023). Because production depends on fish biomass and size structure, fishing can alter the fish contribution to the inorganic carbon cycle (Jennings & Wilson, 2009).

Almost all of this work concerns teleosts. Elasmobranchs (sharks, skates and rays) osmoregulate differently: they retain urea to stay near osmotic

balance with seawater and drink little. In the spiny dogfish (*Squalus acanthias*), the spiral-valve intestine remained close to pH 6.5 after feeding, intestinal bicarbonate was low and little seawater was drunk (Wood *et al.*, 2007), conditions that do not favour teleost-type carbonate precipitation. Whether elasmobranch intestines nevertheless accumulate calcium-rich solids, and what those solids are made of, has not been examined.

SEM–EDX is a practical first step for such work. SEM shows particle morphology, and EDX identifies and quantifies elements in the analysed region. EDX does not identify compounds or crystal structure, so calcium and oxygen together do not prove calcium carbonate, and calcium with phosphorus may indicate calcium phosphate. This study used SEM–EDX to compare intestinal deposits from a teleost, the Indian oil sardine (*Sardinella longiceps*), and an elasmobranch, the Bengal guitarfish (*Rhinobatos annandalei*). The objectives were (1) to isolate and characterise calcium-rich deposits from the intestinal fluid of both fishes, and (2) to compare their elemental composition, particularly calcium.

## 2. MATERIALS AND METHODS

### 2.1 Specimens

Four specimens of *S. longiceps* (Teleostei: Clupeidae) and one ray fish, the Bengal guitarfish *Rhinobatos annandalei* Norman, 1926 (Elasmobranchii: Rhinopristiformes: Rhinobatidae), were obtained fresh, identified from external morphology and transported to the Department of Zoology and Research Centre, Sarah Tucker College, Tirunelveli. The specimens were handled so as to minimise contamination and loss of intestinal contents.

### 2.2 Recovery of intestinal deposits

Each fish was dissected on a clean tray, the abdominal cavity was opened and the intestine was isolated without disturbing its contents. Intestinal fluid was collected into clean containers, separately for each species; the fluid of the four sardines was processed as one composite sample. The fluid was filtered through Whatman No. 1 filter paper, and the retained particulate material was dried in a hot-air oven, cooled, scraped from the paper with a clean spatula and stored in labelled vials.

### 2.3 SEM–EDX analysis

Dried material was mounted on SEM stubs with conductive carbon tape and analysed at the SEM Laboratory, Periyar University, Salem, using a Zeiss scanning electron microscope with an EDAX APEX energy-dispersive X-ray system (Table 1). Secondary-electron images were recorded at 1.89–13.95 kX. Elemental maps and a sum spectrum were acquired from one mapped area per sample, and the software (Smart Quant, ZAF correction) reported weight %, atomic %, net intensity, relative error %, K-ratio and the atomic-number (Z), absorption (A) and fluorescence (F) correction factors for each element. Carbon was not quantified, partly because the carbon tape contributes to the C Kα signal, so all values are normalised to the quantified elements.

**Table 1.** Samples and SEM–EDX acquisition conditions.

| Parameter | Ray fish | Sardine |
|---|---|---|
| Species (group) | *Rhinobatos annandalei* (Elasmobranchii) | *Sardinella longiceps* (Teleostei) |
| Specimens | 1 | 4 (one composite sample) |
| SEM: EHT; working distance | 10 kV; 11.35–11.36 mm | 10 kV; 11.04 mm |
| SEM magnification range | 2.17–13.95 kX | 1.89–13.95 kX |
| EDX: accelerating voltage | 10 kV | 10 kV |
| EDX: map magnification; take-off angle | 3057×; 38.1° | 2406×; 37.8° |
| EDX: live time; amp time; resolution | 81.8 s; 3.84 µs; 127.4 eV | 81.8 s; 3.84 µs; 127.4 eV |

### 2.4 Data analysis

Calcium weight % was the main comparative measure; atomic %, net intensity and the other elements were compared descriptively. Because one sample per species was analysed, no inferential test between species was possible. The analytical uncertainty of each value was estimated from the software's relative error (absolute uncertainty = value × error % / 100), and the uncertainty of the calcium difference was obtained by combining the two in quadrature. Atomic ratios (Ca/P, Mg/Ca, Si/Ca, Al/Si) were calculated from atomic %. As a stoichiometric check, the oxygen expected if every cation were present as a simple oxide ($MgO$, $Al_2O_3$, $SiO_2$, $P_2O_5$, $K_2O$, $CaO$) was subtracted from the measured oxygen; a positive remainder (excess oxygen) indicates oxygen held in other forms, such as carbonate, hydroxyl, water or organic matter. Ca/P ratios were compared with those of hydroxyapatite (1.67) and tricalcium phosphate (1.50).

## 3. RESULTS

### 3.1 Morphology of the deposits

The ray-fish deposit (Figure 1) consisted of a compact base of densely packed ovoid granules about 0.5–1 µm long, on which lay irregular plate-like flakes, smooth straight rods up to more than 10 µm long and stellate aggregates (rosettes) of spindle-shaped

crystallites 2–4 µm long. The rosettes were scattered over the whole surface at low magnification (Figure 1a–c) and resolved at high magnification into radiating crystallites (Figure 1d–f).

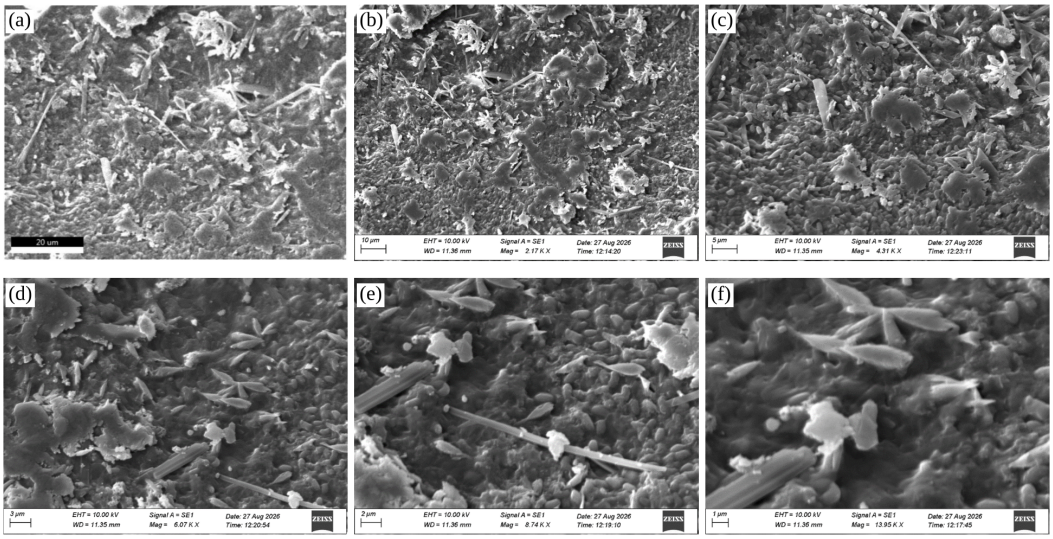



**Figure 1.** SEM micrographs of the ray-fish intestinal deposit: (a) overview, 20 µm bar; (b) 2.17 kX; (c) 4.31 kX; (d) 6.07 kX; (e) 8.74 kX; (f) 13.95 kX.

The sardine deposit (Figure 2) was more heterogeneous: an irregular, crust-like matrix with loose aggregates, fibres and rods (Figure 2a–d), and fragments of diatom frustules with regularly arranged areolae (Figure 2e, f). Rosettes like those of the ray-fish deposit were not seen.

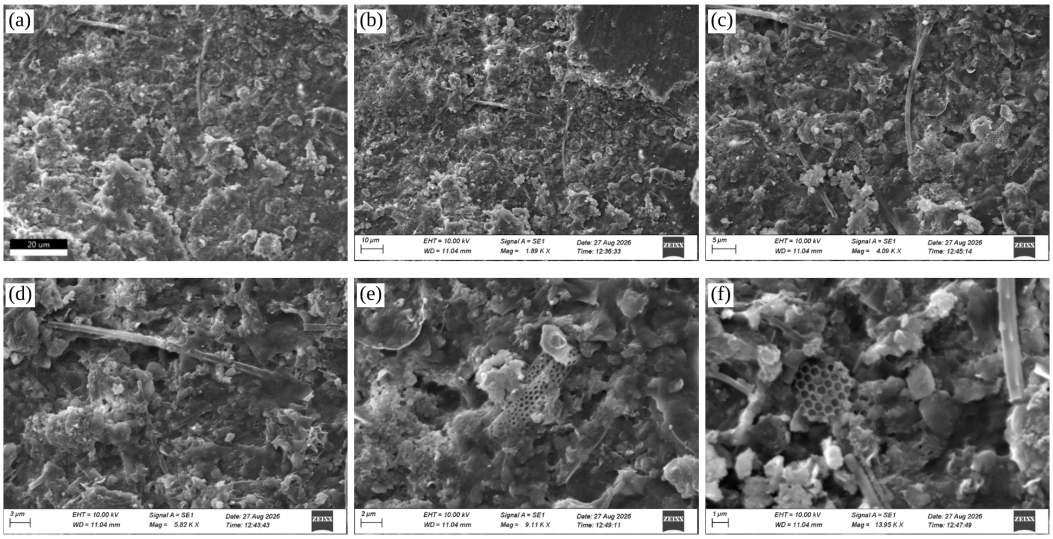



**Figure 2.** SEM micrographs of the sardine intestinal deposit: (a) overview, 20 µm bar; (b) 1.89 kX; (c) 4.09 kX; (d) 5.82 kX; (e) 9.11 kX; (f) 13.95 kX. Diatom frustule fragments are visible in (e) and (f).

### 3.2 Elemental composition

Six elements were quantified in each deposit (Tables 2 and 3; Figure 3). In the ray-fish deposit oxygen was most abundant (47.65 wt.%), followed by calcium (27.47 wt.%) and phosphorus (14.62 wt.%), with silicon (3.52 wt.%), magnesium (3.51 wt.%) and potassium (3.22 wt.%). In the sardine deposit oxygen (48.16 wt.%) was followed by silicon (21.65 wt.%), calcium (11.82 wt.%), aluminium (7.82 wt.%), phosphorus (6.83 wt.%) and magnesium (3.72 wt.%). Relative errors ranged from 4.45% (P) to 22.87% (K) in the ray-fish deposit and from 4.65% (Si) to 9.30% (Ca) in the sardine deposit.

**Table 2.** EDX (Smart Quant) results for the ray-fish intestinal deposit.

| Element | Weight % | Atomic % | Net int. | Error % | K-ratio | Z | A | F |
|---|---|---|---|---|---|---|---|---|
| Oxygen (O) | 47.65 | 66.36 | 154.26 | 9.46 | 0.2050 | 1.0877 | 0.3953 | 1.0000 |
| Magnesium (Mg) | 3.51 | 3.22 | 17.33 | 9.92 | 0.0273 | 0.9893 | 0.7824 | 1.0027 |
| Silicon (Si) | 3.52 | 2.79 | 17.22 | 11.09 | 0.0312 | 0.9676 | 0.9111 | 1.0076 |
| Phosphorus (P) | 14.62 | 10.52 | 52.47 | 4.45 | 0.1279 | 0.9267 | 0.9377 | 1.0065 |
| Potassium (K) | 3.22 | 1.84 | 6.16 | 22.87 | 0.0291 | 0.8841 | 0.9836 | 1.0380 |
| Calcium (Ca) | 27.47 | 15.27 | 39.18 | 7.00 | 0.2445 | 0.8971 | 0.9876 | 1.0043 |

**Table 3.** EDX (Smart Quant) results for the sardine intestinal deposit.

| Element | Weight % | Atomic % | Net int. | Error % | K-ratio | Z | A | F |
|---|---|---|---|---|---|---|---|---|
| Oxygen (O) | 48.16 | 63.51 | 291.61 | 7.38 | 0.2724 | 1.0720 | 0.5276 | 1.0000 |
| Magnesium (Mg) | 3.72 | 3.23 | 27.01 | 8.01 | 0.0299 | 0.9741 | 0.8200 | 1.0043 |
| Aluminium (Al) | 7.82 | 6.11 | 54.28 | 6.23 | 0.0646 | 0.9349 | 0.8778 | 1.0060 |
| Silicon (Si) | 21.65 | 16.26 | 146.33 | 4.65 | 0.1864 | 0.9524 | 0.9009 | 1.0037 |
| Phosphorus (P) | 6.83 | 4.65 | 31.92 | 5.63 | 0.0546 | 0.9120 | 0.8739 | 1.0037 |
| Calcium (Ca) | 11.82 | 6.22 | 23.62 | 9.30 | 0.1035 | 0.8821 | 0.9845 | 1.0082 |

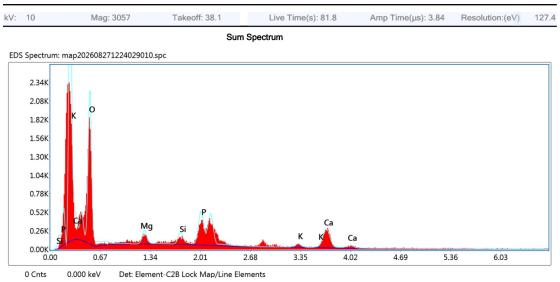
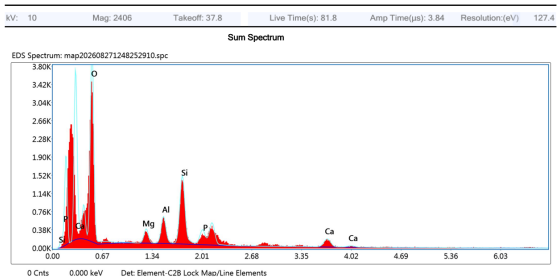



**Figure 3.** (a) EDX sum spectrum of the ray-fish deposit (10 kV).




(b) EDX sum spectrum of the sardine deposit (10 kV). The large peak near 0.28 keV is in the C Kα region.

### 3.3 Comparison of the two deposits

Calcium was 15.65 percentage points higher in the ray-fish deposit (27.47 vs. 11.82 wt.%), a ratio of 2.32 (Table 4, Figure 5). The combined analytical uncertainty of this difference was ±2.21 percentage points, so the difference was about seven times its uncertainty. Calcium atomic % (15.27 vs. 6.22), net intensity (39.18 vs. 23.62) and K-ratio (0.2445 vs. 0.1035) were also higher in the ray-fish deposit. Phosphorus was 2.14 times higher in the ray-fish deposit, whereas silicon was 6.15 times higher in the sardine deposit. Oxygen and magnesium were similar. Aluminium was quantified only in the sardine deposit and potassium only in the ray-fish deposit.

**Table 4.** Comparison of the two deposits (weight % unless stated). — : not quantified in that sample, which does not prove absence.

| Element / measure | Ray fish | Sardine | Difference (ray − sardine) | Ratio (ray/sardine) | Observation |
|---|---|---|---|---|---|
| Oxygen (O) | 47.65 | 48.16 | -0.51 | 0.99 | Similar |
| Calcium (Ca) | 27.47 | 11.82 | +15.65 | 2.32 | Higher in ray fish |
| Phosphorus (P) | 14.62 | 6.83 | +7.79 | 2.14 | Higher in ray fish |
| Silicon (Si) | 3.52 | 21.65 | -18.13 | 0.16 | Higher in sardine |
| Magnesium (Mg) | 3.51 | 3.72 | -0.21 | 0.94 | Similar |
| Aluminium (Al) | — | 7.82 | — | — | Sardine only |
| Potassium (K) | 3.22 | — | — | — | Ray fish only |
| Ca atomic % | 15.27 | 6.22 | +9.05 | 2.45 | Higher in ray fish |
| Ca net intensity | 39.18 | 23.62 | +15.56 | 1.66 | Higher in ray fish |
| Ca error % | 7.00 | 9.30 | — | — | Analytical uncertainty |

### 3.4 Element distribution and diagnostic ratios

Element maps showed calcium, phosphorus and oxygen distributed evenly over the mapped ray-fish area, with patchy calcium enrichment, whereas silicon was dense and widespread in the sardine map (Figure 4). The Ca/P atomic ratio was 1.45 in the ray-fish deposit and 1.34 in the sardine deposit, both below hydroxyapatite (1.67) and close to tricalcium phosphate (1.50); in both deposits, phosphorus was sufficient to bind nearly all the calcium as calcium phosphate (Table 5, Figure 6). The Mg/Ca ratio was 0.21 in the ray-fish deposit and 0.52 in the sardine deposit, and Al/Si in the sardine deposit was 0.38. Measured oxygen exceeded the oxide-stoichiometric value by 15.1 at.% in the ray-fish deposit but by only 0.7 at.% in the sardine deposit.

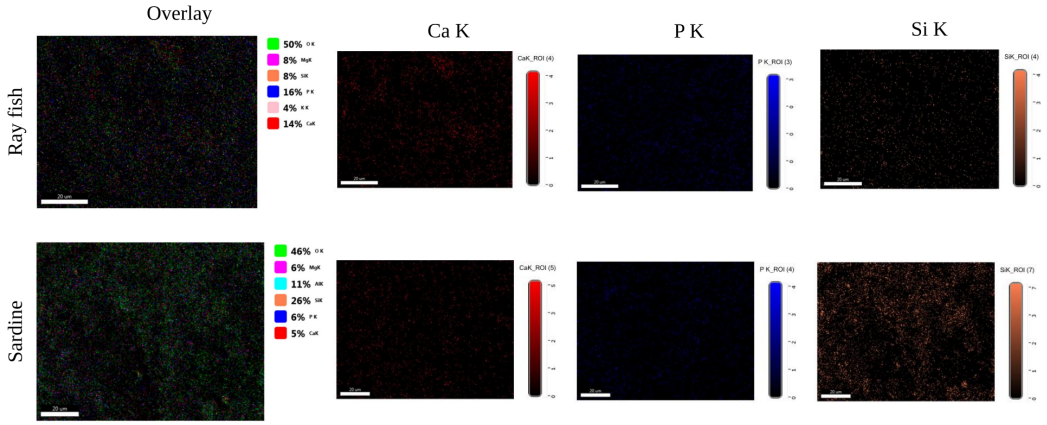



**Figure 4.** EDX element maps of the ray-fish (top) and sardine (bottom) deposits: composite overlay and calcium, phosphorus and silicon maps (scale bars 20 µm).

**Table 5.** Atomic ratios and oxygen balance. Expected O assumes MgO, $Al_2O_3$, $SiO_2$, $P_2O_5$, $K_2O$ and CaO; excess O = measured − expected (atomic %).

| Sample | Ca/P | Mg/Ca | Si/Ca | Al/Si | Expected O | Measured O | Excess O |
|---|---|---|---|---|---|---|---|
| Ray fish | 1.45 | 0.21 | 0.18 | — | 51.29 | 66.36 | 15.07 |
| Sardine | 1.34 | 0.52 | 2.61 | 0.38 | 62.76 | 63.51 | 0.75 |

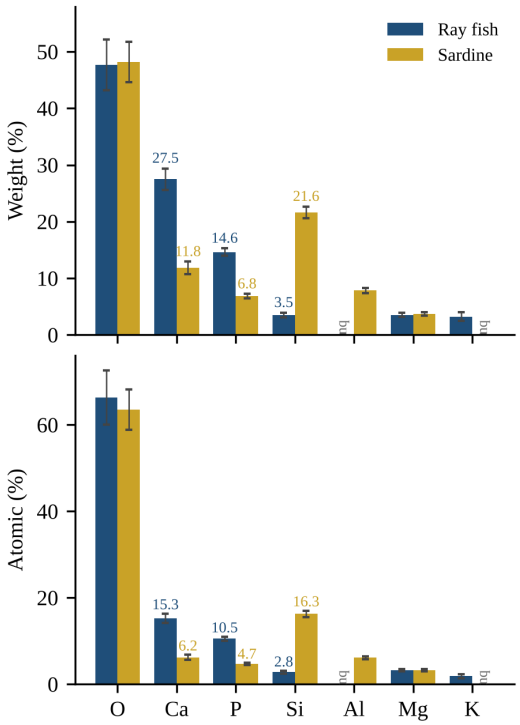



**Figure 5.** Elemental composition by weight and atomic % (bars: analytical uncertainty; nq: not quantified).

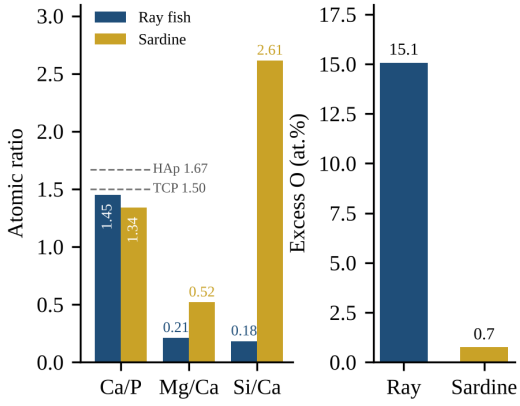



**Figure 6.** Atomic ratios, with the Ca/P of hydroxyapatite (HAp) and tricalcium phosphate (TCP), and excess oxygen.

## 4. DISCUSSION

### 4.1 Calcium in teleost and elasmobranch deposits

Both intestinal deposits contained calcium, and the ray-fish deposit contained 2.3 times more by weight. The difference is far larger than the analytical uncertainty, but it rests on one mapped area of one sample per species, so it describes these two deposits rather than the two fish groups. It is also a difference in composition, not in quantity: EDX percentages do not measure how much deposit a fish forms or excretes. Production estimates such as those of Wilson *et al.* (2009) and Perry *et al.* (2011) combine excretion rates with fish biomass and are not comparable with EDX percentages.

The result is nonetheless notable because of the source. In teleosts, intestinal carbonate forms because the fish drinks seawater and secretes bicarbonate (Wilson & Grosell, 2003; Whittamore *et al.*, 2010). Elasmobranchs drink little and keep the spiral-valve fluid near pH 6.5 with low bicarbonate (Wood *et al.*, 2007), so a calcium-rich intestinal deposit in a ray was not expected from teleost physiology. To our knowledge, this is the first elemental characterisation of such a deposit from an elasmobranch.

### 4.2 Phosphate, carbonate or both?

Phosphorus offers the clearest clue to the mineral form. The Ca/P ratios of 1.45 and 1.34 lie close to tricalcium phosphate and below hydroxyapatite, and in both deposits phosphorus was sufficient to account for nearly all the calcium as calcium phosphate. *R. annandalei* feeds mainly on shrimps, with squid and sciaenid fishes (Purushottama *et al.*, 2020), so fish bone and crustacean cuticle from its prey are a likely source of calcium phosphate. Calcium in these deposits therefore cannot be assigned to carbonate without further evidence.

Two observations nevertheless point to a second phase in the ray-fish deposit. First, its oxygen exceeded oxide stoichiometry by 15.1 at.%, whereas the sardine deposit was almost fully balanced as oxides, silicates and phosphates. Excess oxygen is expected if part of the calcium is present as carbonate, or if the deposit holds hydroxyl, water or organic matter. Second, the rosettes of spindle-shaped crystallites resemble the distinctive crystal morphologies reported for fish-derived carbonates (Salter *et al.*, 2012, 2014). Oxygen quantification at 10 kV involves a large absorption correction (A = 0.395 for oxygen in the ray-fish sample) and is semi-quantitative, so this evidence is indicative only. Fourier-transform infrared spectroscopy (FTIR) and X-ray diffraction (XRD), which distinguished amorphous carbonate in the seabream (Foran *et al.*, 2013) and the mixed phases of Bahamian fish carbonates (Salter *et al.*, 2017), are needed to settle the question.

Magnesium was present at similar levels in both deposits. Fish carbonates are typically magnesium-rich (Wilson *et al.*, 2009; Foran *et al.*, 2013), and high-magnesium calcite dominates in many species (Salter *et al.*, 2017). The higher Mg/Ca ratio of the sardine deposit (0.52 vs. 0.21) is consistent with this, but magnesium in the sardine deposit may also be held in clay minerals or seawater salts, so the ratio cannot be read as evidence of magnesium carbonate.

### 4.3 Silicon and aluminium in the sardine deposit

The dominance of silicon in the sardine deposit is explained by its diet. *S. longiceps* is a plankton feeder in which diatoms make up 57% of stomach contents by index of preponderance, with mud and sand also ingested (Yagnesh & Hitesh, 2022). The diatom frustules seen by SEM confirm a biogenic silica source. Diatom silica contains little aluminium, however, and the Al/Si ratio of 0.38 indicates that aluminosilicate (clay or sediment) particles were also present. The sardine deposit therefore appears to consist largely of ingested plankton and mineral matter, which dilutes any precipitated calcium phase and partly explains its lower calcium percentage.

### 4.4 Implications for carbonate cycling and coral reefs

Fish carbonates matter to the marine inorganic carbon cycle because of their scale, their high magnesium content and their solubility (Wilson *et al.*, 2009), and because production varies with body mass, intestine length, temperature and family (Ghilardi *et al.*, 2023) and with fishing pressure (Jennings & Wilson, 2009). Elasmobranchs are absent from these budgets. If rays and other elasmobranchs form calcium-rich intestinal deposits with a carbonate component, they may be an unrecognised contributor, particularly in the shelf and reef habitats where many species feed. The present data cannot show this: they establish the presence of calcium-rich deposits, not their mineral identity, rate of excretion or fate. Any link to coral reefs is therefore indirect, through the carbonate budgets of reef and shelf sediments rather than coral growth itself.

### 4.5 Limitations and future work

The study analysed one ray fish and one composite sardine sample, each from a single mapped area, so differences between individuals, species and fish groups cannot be separated. Filtration and oven drying may alter amorphous phases, carbon was not quantified, and no procedural blank was analysed to exclude contamination from filter paper or handling. Gut microbes can influence intestinal chemistry (Sullam *et al.*, 2012), but microbial involvement was not examined. Future work should analyse several individuals of each species and several regions per sample, quantify deposit mass, measure intestinal pH and bicarbonate, and identify mineral phases by FTIR and XRD.

## 5. CONCLUSION

Calcium-rich solids were recovered from the intestinal fluid of both a teleost and an elasmobranch. The ray-fish deposit contained 2.3 times more calcium by weight than the sardine deposit (27.47 vs. 11.82 wt.%) and more phosphorus, and showed rosettes of spindle-shaped crystallites and excess oxygen consistent with a carbonate or hydrated phase alongside calcium phosphate. The sardine deposit was dominated by silicon from diatoms and aluminosilicate particles. These findings give a first elemental comparison of teleost and elasmobranch intestinal deposits and show that elasmobranchs deserve inclusion in studies of fish-derived carbonate. Replicated sampling and mineral-phase analysis are needed before their contribution to marine carbonate cycling and reef sediment budgets can be assessed.

## REFERENCES

Foran, E., Weiner, S., & Fine, M. (2013). Biogenic fish-gut calcium carbonate is a stable amorphous phase in the gilt-head seabream, *Sparus aurata*. *Scientific Reports*, 3, 1700.

Ghilardi, M., Salter, M. A., Parravicini, V., Ferse, S. C. A., Rixen, T., Wild, C., Birkicht, M., Perry, C. T., Berry, A., Wilson, R. W., Mouillot, D., & Bejarano, S. (2023). Temperature, species identity and morphological traits predict carbonate excretion and mineralogy in tropical reef fishes. *Nature Communications*, 14, 985. https://doi.org/10.1038/s41467-023-36617-7

Jennings, S., & Wilson, R. W. (2009). Fishing impacts on the marine inorganic carbon cycle. *Journal of Applied Ecology*, 46(5), 976–982.

Perry, C. T., Salter, M. A., Harborne, A. R., Crowley, S. F., Jelks, H. L., & Wilson, R. W. (2011). Fish as major carbonate mud producers and missing components of the tropical carbonate factory. *Proceedings of the National Academy of Sciences*, 108(10), 3865–3869. https://doi.org/10.1073/pnas.1015895108

Purushottama, G. B., Ramasubramanian, V., Akhilesh, K. V., Raje Thakurdas, S. G., Kizhakudan, S. J., & Zacharia, P. U. (2020). Biological observations on the Bengal guitarfish *Rhinobatos annandalei* Norman, 1926 from the Eastern Arabian Sea, India. *Indian Journal of Fisheries*, 67(2), 23–34. https://doi.org/10.21077/ijf.2019.67.2.94482-04

Salter, M. A., Harborne, A. R., Perry, C. T., & Wilson, R. W. (2017). Phase heterogeneity in carbonate production by marine fish influences their roles in sediment generation and the inorganic carbon cycle. *Scientific Reports*, 7, 765. https://doi.org/10.1038/s41598-017-00787-4

Salter, M. A., Perry, C. T., & Wilson, R. W. (2012). Production of mud-grade carbonates by marine fish: Crystalline products and their sedimentary significance. *Sedimentology*, 59(7), 2172–2198. https://doi.org/10.1111/j.1365-3091.2012.01339.x

Salter, M. A., Perry, C. T., & Wilson, R. W. (2014). Size fraction analysis of fish-derived carbonates in shallow sub-tropical marine environments and a potentially unrecognised origin for peloidal carbonates. *Sedimentary Geology*, 314, 17–30. https://doi.org/10.1016/j.sedgeo.2014.10.005

Sullam, K. E., Essinger, S. D., Lozupone, C. A., O'Connor, M. P., Rosen, G. L., Knight, R., Kilham, S. S. & Russell, J. A. (2012). Environmental and ecological

factors that shape the gut bacterial communities of fish: a meta-analysis. *Molecular Ecology*, 21, 3363–3378.

Whittamore, J. M., Cooper, C. A., & Wilson, R. W. (2010). $HCO_3^-$ secretion and $CaCO_3$ precipitation play major roles in intestinal water absorption in marine teleost fish *in vivo*. *American Journal of Physiology – Regulatory, Integrative and Comparative Physiology*, 298, R877–R886.

Wilson, R. W., & Grosell, M. (2003). Intestinal bicarbonate secretion in marine teleost fish: Source of bicarbonate, pH sensitivity, and consequences for whole animal acid–base and calcium homeostasis. *Biochimica et Biophysica Acta – Biomembranes*, 1618(2), 163–174.

Wilson, R. W., Millero, F. J., Taylor, J. R., Walsh, P. J., Christensen, V., Jennings, S., & Grosell, M. (2009). Contribution of fish to the marine inorganic carbon cycle. *Science*, 323(5912), 359–362.

Wood, C. M., Kajimura, M., Bucking, C., & Walsh, P. J. (2007). Osmoregulation, ionoregulation and acid–base regulation by the gastrointestinal tract after feeding in the elasmobranch (*Squalus acanthias*). *Journal of Experimental Biology*, 210(8), 1335–1349. https://doi.org/10.1242/jeb.02736

Yagnesh, M., & Hitesh, K. (2022). Food and feeding habits of *Sardinella longiceps* Valenciennes, 1847 caught along Veraval coast of Gujarat. *Indian Journal of Fisheries*, 69(2), 56–65. https://doi.org/10.21077/ijf.2022.69.2.108213-07